Practical design and performance of the stressed-lap polishing tool

S. C. West, H. M. Martin, R. H. Nagel, R. S. Young, W. B. Davison, T. J. Trebisky, S. T. DeRigne, and B. B. Hille

We present an overview of the engineering design and empirical performance of four stressed-lap polishing tools developed at the University of Arizona. Descriptions of the electromechanical actuators, servo systems, computer interfacing, and attachment of the lap to the polishing machine are provided. The empirical performance of a representative tool is discussed in terms of accuracy, repeatability, and hysteresis. Finally, we estimate the statistical likelihood of aluminum lap-plate failure through a metal-fatigue analysis for a worst-case stress-cycling situation.

Key words: Optical fabrication, polishing.

1. Introduction

The research effort at the Steward Observatory Mirror Laboratory led to the development of a new deformable large-tool polishing technique that has had great success in the past few years. We call it the stressed-lap technique, and it is one solution to the fundamental problem of shape misfit that occurs for large polishing tools on highly aspheric optical surfaces. For example, a rigid passive lap cannot maintain an accurate fit to a paraboloidal surface because of the variations in curvature across the surface. The decrease in curvature from vertex to edge causes a misfit with the form of defocus, the unequal radial and tangential curvatures cause astigmatic misfit, and the variation of radial curvature across the lap face causes comatic misfit. In principle, though, a large stiff tool is advantageous because it produces high glass-removal rates and natural smoothing over a wide range of spatial frequencies. The stressed lap permits the use of a large stiff tool on highly aspheric surfaces because its shape is actively changed as it is moved over the surface. The shape changes are induced in a large circular plate through the application of bending and twisting edge moments.

To date, the stressed-lap technique has successfully polished several borosilicate honeycomb primary mirrors to better than 22-nm rms surface error[1–5]: (a) the 1.8-m $f/1.0$ Vatican Advanced Technology Telescope (VATT), (b) the 3.5-m $f/1.5$ U.S. Air Force Phillips Laboratory Telescope, (c) the 3.5-m $f/1.75$ Astrophysical Consortium Telescope, and (d) the 3.5-m $f/1.75$ Wisconsin, Indiana, Yale, National Optical Astronomy Observatories Telescope.

This paper summarizes the engineering efforts that went into the development of the stressed lap (a forthcoming paper will discuss the principles and conceptual design of the stressed lap). Section 2 provides a basic description of the mechanical, servo, and interfacing systems as well as the empirical performance of the tool, including shape calibration, reproducibility, and hysteresis. Section 3 discusses attachment to the polishing machine. Section 4 gives a fatigue analysis of the lap plate used to estimate lifetime and aid in the selection of an appropriate aluminum alloy.

2. Basic Description

One of the basic goals of the stressed lap is for the computer to control tool deformation in a manner that is transparent to the optician, so that for practical purposes the optician can polish a highly aspheric surface as if he or she were polishing a sphere. A relatively complex control system for the stressed lap allows the optician to concentrate on figuring the mirror without regard to its asphericity. The computer continuously reads the lap's position and orientation with respect to the mirror with encoders. This information, plus the mirror surface geometry, permits the computer to control the lap shape independently as it moves.

The authors are with the Steward Observatory, University of Arizona, Tucson, Arizona 85721.

Received 28 February 1994.
0003-6935/94/348094-07$06.00/0.

Combined with high mechanical stiffness, low-noise servo electronics, relatively high-response bandwidth, and shape repeatability free of hysteresis, the stressed lap in principle removes much of the complication of polishing a highly aspheric optic. In addition, early polishing experiments proved that the attachment of the lap to the polishing machine was critical to the control of unwanted pressure gradients across the lap face, and that varying the axial polishing pressure in proportion to local surface erorrs increased the convergence rate. This section describes the mechanical and electrical designs we incorporated into the stressed lap to achieve these goals.

A. Mechanical

The stressed lap consists of a solid circular aluminum plate with steel tubes attached to the perimeter. Electromechanical actuators create bending and twisting moments at the edge of the plate by applying forces to the tops of the tubes. The forces are transmitted by steel bands in tension. Figure 1 shows a schematic side view of a stressed lap with one such actuator. As the top view in Fig. 2 shows, each tube contains one actuator and also serves as the termination for the band of another actuator. With the bands arranged in triangles as shown, the necessary bending and twisting moments can be applied. The mechanical components of an actuator consist of a torque motor, ball screw, lever arm, and linkage. The tension in each band is measured with a load cell at the termination point, and this tension serves as the servo feedback signal to control motor torque. A preload tension is applied to the entire set of bands so that they remain in tension anywhere on the mirror, thus eliminating backlash from the mechanical force system at the transition between tension and compression. The discrete application of moments causes some scalloping of the plate near the actuators, so the active polishing area is constrained to be the inner 80% diameter of the plate.

Table 1 summarizes the properties of the stressed laps built to date and gives a side view of each actuator design. The first stressed lap we built had actuators based on the design shown last in the table and was used to polish the 1.8-m $f/1.0$ primary mirror for the VATT. The force feedback system was based on sensing the deflection of a steel beam with a linearly variable differential transformer. Although the lap was adequate to finish the mirror, the hysteresis of this feedback system led to unacceptable shape errors, and considerable polishing from small hand tools was required to reach the final surface figure accuracy of 17 nm rms. This lap has since been decommissioned in favor of designs that incorporate load cells to measure band tension, thereby improving the shape accuracy and repeatability at least sevenfold. The 1.2-m lap has been used to polish three 3.5-m mirrors, and it will be the primary tool used to polish all of our 6.5-m and 8.4-m primary mirrors. The 30-cm and new 60-cm tools will be used in our secondary-mirror polishing program.

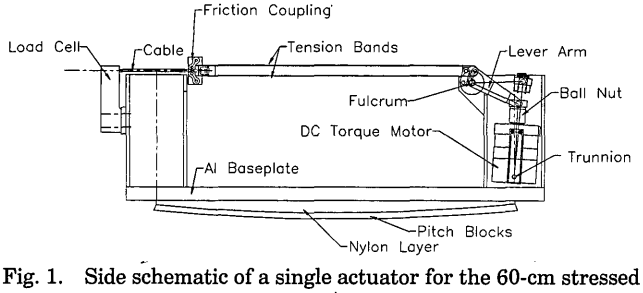

Fig. 1. Side schematic of a single actuator for the 60-cm stressed lap. By the application of tension to the steel bands with an electromechanical actuator, a bending moment is produced in the plate. Motor torque is converted into linear force at the bands by a ball screw and a lever arm. A parallelogram linkage attached to the fulcrum ensures not only that the force application height is constant throughout the dynamic range, but also that the tension bands do not twist. The plastic layer gives the pitch surface the proper average curvature.

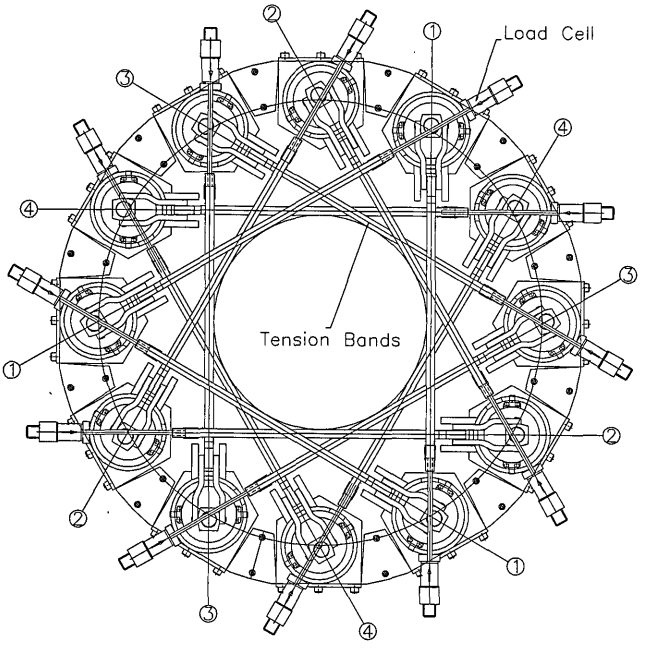

Fig. 2. Top view of the 60-cm stressed lap; 12 actuators are attached to the periphery of the plate, and twisting and bending moments are produced by the arrangement of the tension bands in sets of equilateral triangles.

B. Electrical

An actuator is a constant force device that is position and stroke independent. Changing the lap shape is accomplished by changing the force distribution that all actuators apply to the lap plate. The electrical components consist of a dc torque motor driven by a pulsed-wave modulated servo amplifier, an analog proportional integral (PI) stage, and the feedback load cell force signal. A dc tachometer provides torque stabilization. In real time, the servo rejects unwanted moments produced by the influence of neighboring actuators and those caused by mirror contact when polishing.

Table 1. Stressed Laps Built to Date

Parameters	Measurements	Actuator Schematic[a]
Max. polishing diameter (m)	1.2	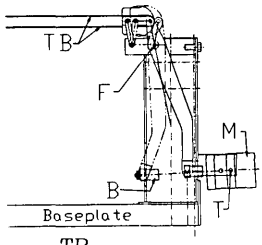
No. of actuators	18	
Peak bending torque (*Nm*)	3400	
Feedback type	Load cell	
Plate thickness (cm)	5.21	
Max. polishing diameter (m)	0.6	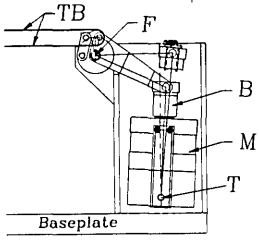
No. of actuators	12	
Peak bending torque (*Nm*)	1380	
Feedback type	Load cell	
Plate thickness (cm)	2.54	
Max. polishing diameter (m)	0.3	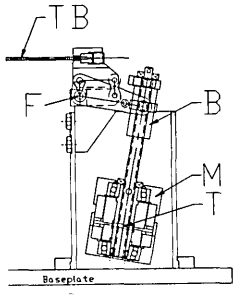
No. of actuators	12	
Peak bending torque (*Nm*)	340	
Feedback type	Load cell	
Plate thickness (cm)	1.27	
Max. polishing diameter (m)	0.6	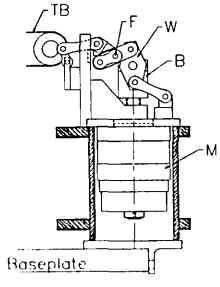
No. of actuators	12	
Peak bending torque (*Nm*)	960	
Feedback type	Beam deflection	
Plate thickness (cm)	2.54	

[a]TB, tension band; F, fulcrum; M, motor; B, ball nut; T, trunnion; W, watts linkage. The relative scale of each drawing is different.

A force command is issued to an actuator by the placement of the data (force value) and the address (actuator number) onto a bus that is connected to all actuators. An address decoder selects the actuator, and a strobe latches the data onto the appropriate tension servo. The schematic is shown in Fig. 3. During operation, a 25-MHz 68030 computer running VxWorks (Wind River Systems, Inc.) continually reads the polishing machine encoders and serially updates individual actuators at a rate of 22 kHz (1.8-kHz shape-update rate of a lap with 12 actuators). A system diagram is shown in Fig. 4.

C. Shape Calibration

The relationship between the lap shape and actuator forces is determined with a set of linearly variable

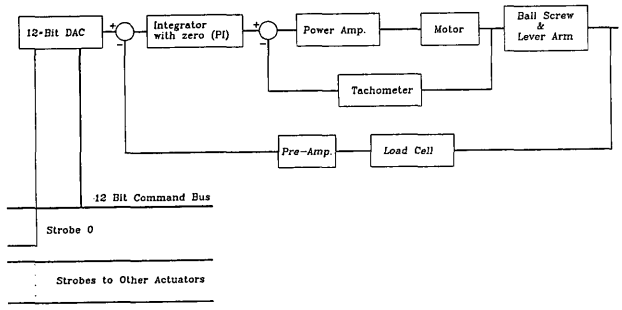

Fig. 3. Schematic for the stressed-lap tension servo system. Force commands are loaded into each actuator by the strobing of a 12-bit word into a registered digitial-to-analog coverter (DAC) from a data bus. The shape-update rate is over 1 kHz. The servo bandwidth and damping coefficient are set to yield a maximum 0.1° shape-phase lag error at 10-rpm lap rotation rate.

differential transformer sensors. The lower surface of the lap plate is brought into contact with the sensor matrix by means of a three-point kinematic attachment. Given the geometry of the optical surface, a position and orientation for the lap, and feedback from the contact sensors, the computer uses an iterative least-squares method to determine the best set of actuator forces that yield the correct plate shape. For nearly paraboloidal optical surfaces, analytic solutions similar to those by Lubliner and Nelson[6] are used to calculate the desired sensor displacements. In this case, an analytic solution is tractable because the sag equation has a simple form. For arbitrary conic, the sag equation is transformed into

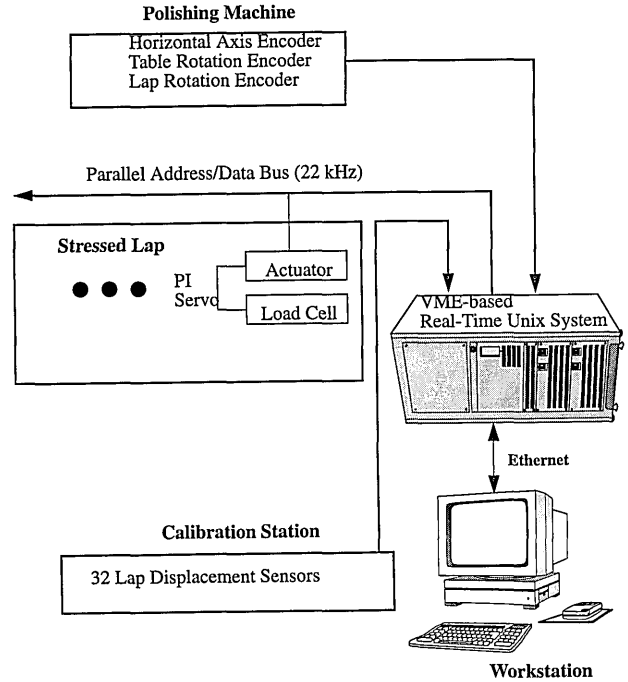

Fig. 4. Electronic system diagram of stressed-lap operation. Lap shapes are determined at the calibration station and used to generate a high-density lookup table of actuator value versus mirror position. During polishing, the VME-based computer reads the encoders on the polishing machine and updates the lap shape at 1-kHz rates with the lookup table.

local coordinates centered at the lap position through the use of, e.g., the Levenberg–Marquardt solver built into MATHCAD (MathSoft, Inc.).

D. Empirical Performance

Figure 5 shows the typical shape accuracy obtained during calibration of the 1.2-m stressed lap on the U.S. Air Force 3.5-m $f/1.5$ primary mirror along with the errors seen when we attempt to reproduce these shapes. The lower part of the figure shows the corresponding decomposition of the bending moments into coma, defocus, and astigmatism. Bending hysteresis resulting from all possible sources is displayed in Fig. 6. Hysteresis and shape repeatability were not obtained with the lap actually in contact with the mirror, but rather by placing the lap on the calibration fixture and simulating the movement. The time stability of the lap servo system and associated electronics are shown in Fig. 7.

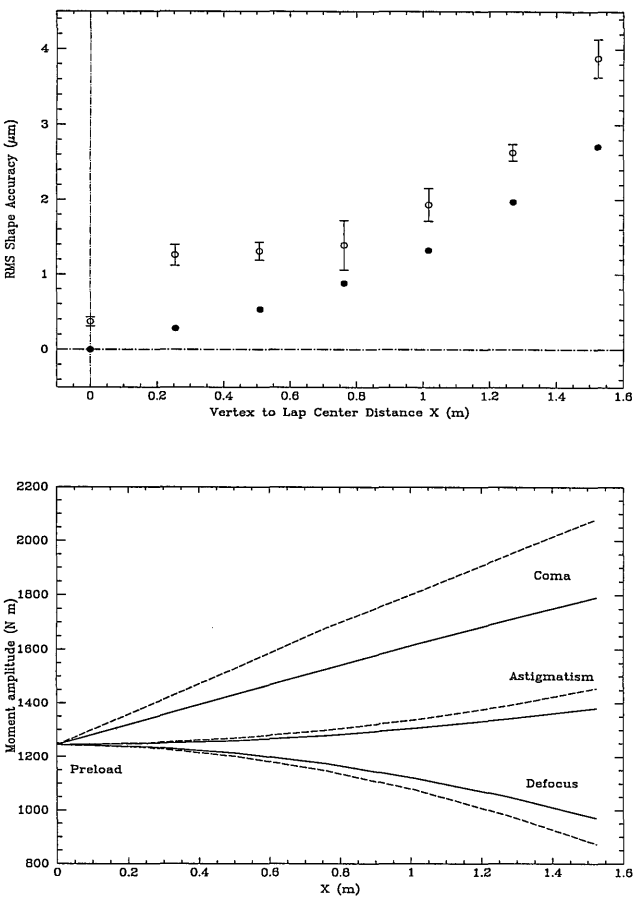

Fig. 5. Upper plot shows the shape accuracy of the 1.2-m stressed lap produced by calibration for the 3.5-m $f/1.5$ U.S. Air Force mirror (solid points) versus the distance of the lap center from the vertex of the mirror (X). Also shown are the rms errors that are produced by the random accessment of these shapes and their comparison with the calibration. This is the most severe test of shape reproducibility and includes all effects from mechanical hysteresis, kinematic attachment, and servo errors. The lower plot shows the corresponding moment amplitudes (peak mode force times the post height) introduced by the actuators for defocus, coma, and astigmatism. At $X = 1.52$ m, these correspond to 360, 129, and 170 μm of plate deflection, respectively. Plate theory (solid curve) underestimates the actual moments (dashed curves) because of plate stiffening at the lap periphery caused by the steel attachment brackets of the actuators (shown in Fig. 2).

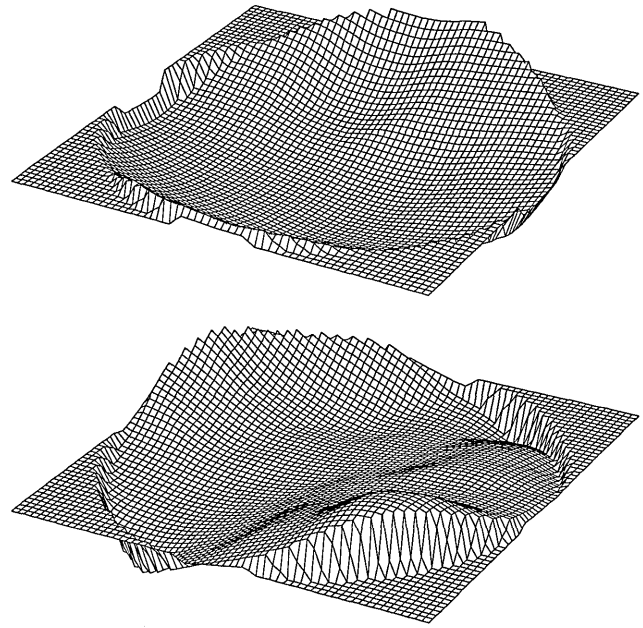

Fig. 6. Highly exaggerated stressed-lap hysteresis plots derived from the data set used to produce Fig. 5. In each case a contour map is computed by the subtraction of two shapes derived from moving the lap in opposite directions. The top plot shows the difference map produced by moving the lap from the center to the edge of the mirror and back again with no rotation. The two shapes produced at the 50% zone of the mirror are subtracted and displayed. The bottom plot shows hysteresis produced at the mirror edge by subtracting shapes produced by rotating the lap in opposite directions. In each case the difference maps have errors of less than 1.5 μm rms and 4 μm peak to valley over the full 1.2-m diameter of the lap.

3. Attachment to the Polishing Machine

In addition to the internal bending stresses applied to the lap plate by its actuators, the lap experiences external forces induced by the polishing machine and the mirror. The machine applies substantial lateral forces to translate and rotate the lap, and it may also apply varying forces normal to the plate as part of the figuring process. These external forces produce reactions in the form of varying pressure gradients across the polishing surface. Several effects tend to produce unwanted pressure gradients that can interfere with figuring. Running the lap off of the mirror edge induces an overturning moment into the lap plate and causes the plate to distort. On a sloped surface, the stressed lap's high center of gravity (produced by tall actuators) induces overturning moments into the plate. A lateral force used to translate the lap across the mirror surface that is applied out of plane with the actual dragging surface of the pitch blocks produces unwanted pressure gradients. Friction in the polishing machine can produce pressure hysteresis in parts of the polishing strokes.

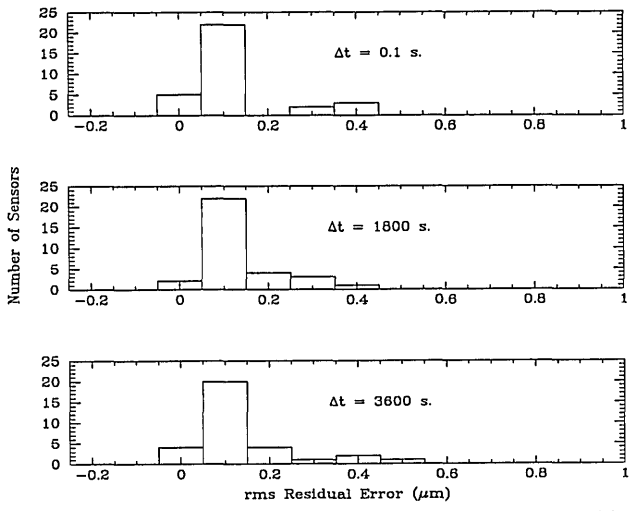

Fig. 7. One measure of the time stability of the stressed-lap tension servo system shows histograms of the sensor rms errors relative to the reference shape at $t = 0$. Any electronic or uncompensated mechanical drift will look like a shape change and cause the error distribution to translate along the abscissa. Clearly, instability of the stressed-lap electronics is not measurable in 1-h time periods.

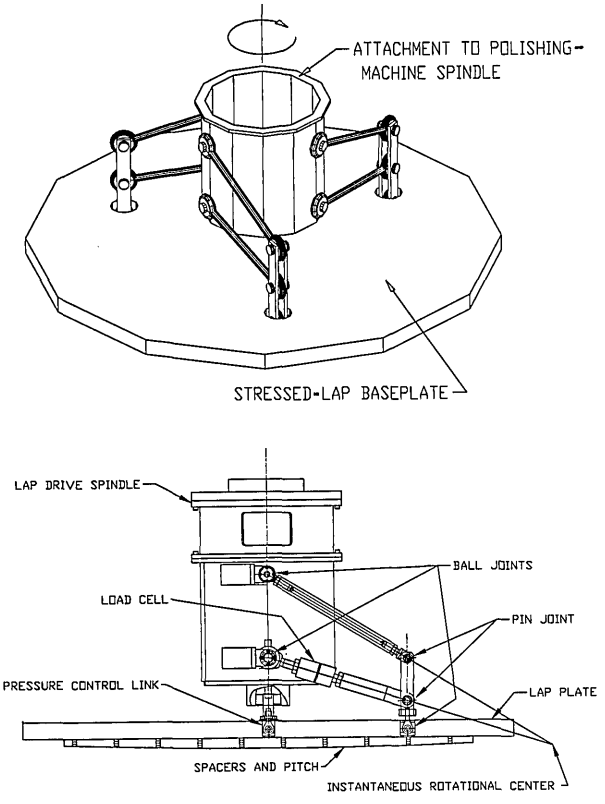

Fig. 8. Two views of the passive mechanical linkage used to connect the 1.2-m stressed lap to the polishing-machine spindle. The upper view depicts the layout of the three four-bar linkages and shows how torque is transmitted to the lap plate. The lower view shows the details of a single four-bar linkage. Each linkage is connected to the midplane of the lap plate by a ball joint that precludes bending moments, produced by the lateral dragging force, from deforming the plate. The linkages passively eliminate unwanted pressure gradients caused by drag and accommodate tilt and piston as the lap is moved over the surface of the mirror. Although the linkages partially compensate for overturning moments, complete cancellation requires active control.

Experience has shown that one need not address all of these points in order to polish a mirror successfully. For example, the stressed lap used for the VATT 1.8-m $f/1.0$ mirror had a ball-joint connection at the center of the lap plate and a simple actively controlled spring arrangement to compensate overturning moments. It had no compensation for pressure gradients caused by lateral drag. In contrast, the 3.5-m $f/1.5$ and $f/1.75$ mirrors were all polished to near 20-nm rms surface errors with a mechanical linkage that eliminated drag-induced pressure gradients but only partially compensated for overturning moments.

The ideal connection between the lap and polishing machine contains the following ingredients. The lateral force used to move the lap should be applied near the glass-to-lap interface to eliminate drag-induced pressure gradients. The linkage through which the lateral force is applied should not transmit any spurious moments into the lap plate that would cause it to deform. The linkage should passively float through a height equal to the sag of the optic as well as accommodate changes in slope up to 15° (for an $f/1.0$ paraboloid). Last, it should provide active compensation of spurious external moments.

Figure 8 depicts the mechanical linkage (used with the 3.5-m mirrors) that passively eliminates deforming plate moments and pressure gradients associated with dragging the lap over the surface of the mirror. It also provides partial compensation of overturning moments. It consists of three four-bar linkages that have their instantaneous rotational centers near the glass-to-lap interface. The instantaneous rotational center is the projected intersection of the two arms on each linkage, and no unwanted moment is introduced as long as the plane defined by these points coincides with the actual dragging surface. As shown in the upper figure, one transmits torque to the plate by attaching the three linkages tangent to a large hub, which itself connects to the polishing-machine spindle. Axial lap pressure is regulated in proportion to the local surface figure error with a pressure transducer attached to the plate center (shown in lower figure).

Future polishing of all primary and secondary mirrors will incorporate real-time application of axial forces into the four-bar linkages. With three axial forces controlled independently, we can apply any combination of net axial force and moments about the two lateral axes. In this way undesired pressure gradients can be eliminated, and desired pressure gradients can be applied to adjust the glass-removal profile according to the measured surface errors.

4. Plate Fatigue and Alloy Selection

Fatigue is the gradual deterioration of a material that is subjected to repeated loading. Clearly this is an important issue for stressed-lap polishing. To evaluate the statistical likelihood of lap-plate failure, we

performed an analysis of lifetime for the most severe polishing situation we could envision: a 2.2-m-diameter, 10-cm-thick plate used to polish both the 6.5-m $f/1.25$ Multiple Mirror Telescope Conversion (MMTC) and the 8.4-m $f/1.14$ Large Binocular Telescope (LBT) primary mirrors.

Table 2 lists the strength properties of Al alloys and clearly illustrates that wrought Al is much stronger than cast. Alloys are listed in descending order of ultimate strength.

For cyclic stresses, the fatigue strength, S_f, depends on the number of stress cycles, N, combined with modification factors for the material, its machining, and its environment. A plot of N versus fatigue strength is called an SN diagram. The ultimate strength, S_{ut}, of a material is the fatigue strength for $N = 1/2$. For $N = 10^3$–10^8, Fig. 9 shows the resulting SN diagrams for 7075-T6 and 6061-T6 Al (which we consider to be the most readily available of the wrought alloys in large ingots). Solid curves show the respective unmodified fatigue strengths, and dotted curves show the modified strengths for the stressed-lap plate. Assumptions used in the deviation of these curves are given elsewhere.[7,8]

The actual fatigue limit of a stressed-lap plate depends on the number of stress cyles, N, the mean stress, σ_m, and the amplitude of stress variation, σ_a. A conservative estimate for sinusoidal cyclic fatigue failure is based on the Goodman diagram shown in Fig. 10. The diagram relates the mean stress and the alternating stress amplitude where fatigue failure occurs and depends on the number of stress cycles. One obtains the Goodman criterion by drawing a straight line from mean stress $\sigma_m = S_{ut}$ to an alternating stress amplitude of $\sigma_a = S_f(N)$ and requiring that the stresses be kept below this line. This criterion is clearly accurate at the end points and has been shown to be conservative in between. Therefore if $\sigma_m = 0$, fatigue failure is avoided for $\sigma_a < S_f$. If $\sigma_m = S_{ut}$, then no alternating amplitude is allowed. Goodman relations using the modified fatigue strengths of Fig. 9 (at $N = 10^6$ and $N = 10^7$) are shown for both 7075 and 6061 alloys.

One approximates the stressed lap on this diagram by considering two simplified types of alternating stresses: (a) the cycling that occurs for a point on the edge of the plate as the lap rotates near the edge of the mirror, and (b) stress cycling that occurs near the center of the plate as the lap is translated from mirror vertex to edge. A simple finite-element model of the plate was constructed with shell elements, and the optical shape displacements were input directly onto the nodes of the model for various lap positions (alternatively, the stress could be calculated analytically[6]). The total bending of the plate consists of two parts: (a) the off-axis shape subtracted from the vertex shape, and (b) a spherical preload that acts as the reference shape at the vertex. The preload must have curvature because the lap flattens away from the vertex, and our actuators are not bidirectional. Figure 11 shows the modeled azimuthal variation of plate stress near the edge of a 2.2-m lap for the 6.5-m $f/1.25$ (MMTC) and 8.4-m $f/1.14$ (LBT) mirrors. The variable X signifies the distance of the lap center from the mirror vertex. Both models use identical preload curvatures ($X = 0$ m). It is interesting to note that the highest stress is always produced by the

Table 2. Strength Properties of Various Al Alloys

	Ultimate Strength		Yield Strength		Fatigue Strength at 50 Mcycles	
Alloy/Temper	kpsi	MPa	kpsi	MPa	kpsi	MPa
7075-T6 (wrought)	82	565	72	496	24	165
2014-T6 (wrought)	70	483	60	414	18	124
2024-T4 (wrought)	68	469	48	331	20	138
2219-T87 (wrought)	61	421	49	338	?	?
6061-T6 (wrought)	45	310	40	276	13.5	93
Typical (cast)	35	241	25	172	9	62
K-100 (cast)	33	228	22	152	?	?

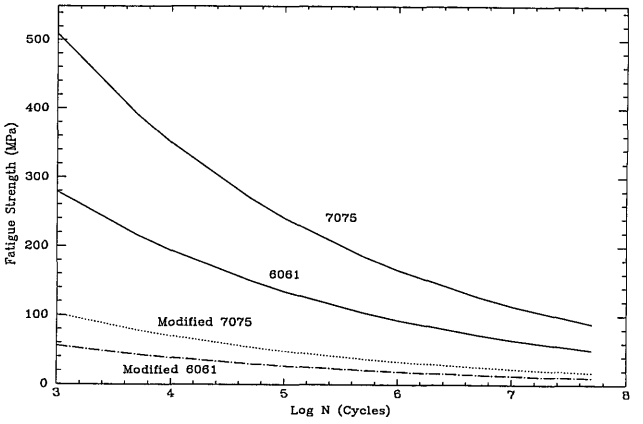

Fig. 9. SN diagrams for 7075 and 6061 Al alloys with T6 temper. The solid curves show the unmodified fatigue strength, and the dashed curves show fatigue strength modified appropriately for the plate machining, surface finish, and environment.

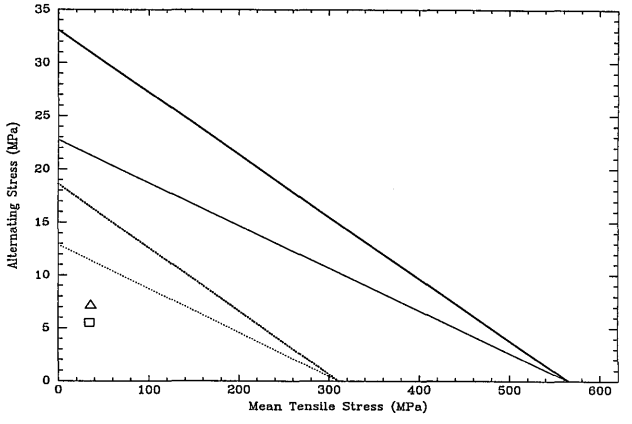

Fig. 10. Modified Goodman relations for Al alloys of 7075-T6 (solid curves) and 6061-T6 (dashed curves) for log $N = 6$ (thick curves) and log $N = 7$ (thin curves). The alternating and mean stresses of a 2.2-m plate are shown for the center (triangle) and periphery (square) of the plate. They were determined by a finite-element analysis that modeled polishing strokes.

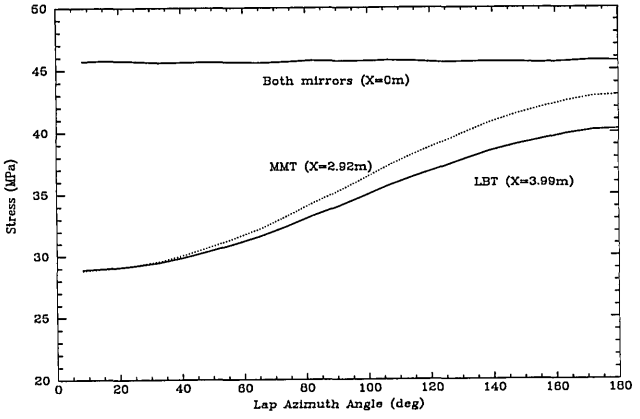

Fig. 11. Azimuthal variation of the peripheral plate stresses for models of a 2.2-m stressed-lap plate on the Multiple Mirror Telescope (MMT) and Columbus primary mirrors as a function of the distance of the lap center from the mirror vertex (X). The mirror vertex is toward an azimuth of 180°. The upper curve represents the preload stress, and the lower two curves show plate stress around the periphery when the lap center is near the mirror edge.

preload, because at any other location on the mirror, the plate curvature is smaller (even though the forces on some actuators are larger). In addition, the stress at the center of the plate shows a range of 45.7 MPa at the vertex to 34.1 and 35.2 MPa near the edges of the LBT and MMTC mirrors, respectively. The safety (or confidence) factor $[S_f(N)/\sigma_a]$ signifies how much greater the fatigue strength is than the applied stress amplitude. The safety factors for both the center and edge at $N = 10^6$ are approximately 6 and 3.4 for 7075 and 6061, respectively, and they narrow to 4 and 2.4 for $N = 10^7$.

One can estimate the lifetime of the plate by first estimating N for polishing one mirror. We assume that the lap, on average, rotates at 5 rpm and is completely translated on the mirror from vertex to edge at 0.5 cycles/min, and that completing one mirror requires 320 h of polishing and loose-abrasive grinding combined. These assumptions lead to $N = 10^5$ rotations and $N = 10^4$ translations per mirror. Therefore for a total of 10^6 stress cycles, we can polish up to ten $f/1$-type mirrors by using a lap that is 1/3 the diameter of the mirror with a reasonable safety margin.

5. Conclusion

We have shown that constructing a polishing tool with dynamically controllable off-axis optical shapes can be accomplished with relatively straightforward mechanical and electrical systems. These laps have routinely produced 20-nm rms optical surfaces on large aspheric telescope primary mirrors with speeds ranging from $f/1.75$ to $f/1.0$. Shape repeatability errors are kept below 4 μm rms for tools as large as 1/3 of the diameter of the optic being polished. Even after polishing ten $f/1.0$ aspheres, a 7075-T6 aluminum plate provides a comfortable safety margin against cyclic fatigue failure. Current stressed-lap research not reported here includes the active control of pressure gradients of the tool during polishing as well as experiments to optimize the convergence rate of the technique and the accurate prediction of glass-removal profiles.

We acknowledge the excellent work of the Steward Observatory technical division, without whose help the implementation of the stressed lap would have been compromised. D. Murgiuc contributed most of the design and drafting required. J. Urban manufactured the lap actuators by using a computerized milling machine. S. Schaller helped produce the software skeleton for the control of the lap. V. Moreno flawlessly wired each lap. Technical support for innumerable details came from K. Duffek, R. Kraff, B. Phillips, B. McClendon, M. Orr, I. Lanum, R. Miller, and G. Weir. This research was funded by National Science Foundation cooperative agreement AST 89011701 and a U.S. Air Force Phillips Laboratory contract.

References

1. H. M. Martin, J. R. P. Angel, and A. Y. S. Cheng, "Use of an actively stressed lap to polish a 1.8-m paraboloid," in *Proceedings of the European Southern Observatory Conference on Very Large Telescopes and Their Instrumentation,* M. H. Ulrich, ed. (European Southern Observatory, Garching-bei-Muchen, Germany, 1988), p. 353.
2. H. M. Martin, D. S. Anderson, J. R. P. Angel, R. H. Nagel, S. C. West, and R. S. Young, "Progress in the stressed-lap polishing of a 1.8-m $f/1$ mirror," in *Advanced Technology Optical Telescopes IV,* L. D. Barr, ed., Proc. Soc. Photo-Opt. Instrum. Eng. **1236,** 682–690 (1990).
3. D. S. Anderson, J. R. P. Angel, J. H. Burge, W. B. Davison, S. T. DeRigne, B. B. Hille, D. A. Ketelsen, W. C. Kittrell, H. M. Martin, R. H. Nagel, T. J. Trebisky, S. C. West, and R. S. Young, "Stressed-lap polishing of 3.5-m $f/1.5$ and 1.8-m $f/1.0$ mirrors," in *Advanced Optical Manufacturing and Testing II,* V. J. Doherty, ed., Proc. Soc. Photo-Opt. Instrum. Eng. **1531,** 260–269 (1991).
4. D. S. Anderson, J. H. Burge, D. A. Ketelsen, H. M. Martin, S. C. West, G. Poczulp, J. Richardson, and W. Wong, "Fabrication and testing of the 3.5-m, $f/1.75$ WIYN primary mirror," in *Fabrication and Testing of Large Optics,* V. J. Doherty, ed., Proc. Soc. Photo-Opt. Instrum. Eng. **1994,** 193–207 (1993).
5. S. C. West, J. H. Burge, R. S. Young, D. S. Anderson, C. Murgiuc, D. A. Ketelsen, and H. M. Martin, "Optical metrology for two large highly aspheric telescope mirrors," Appl. Opt. **31,** 7191–7197 (1992).
6. J. Lubliner and J. E. Nelson, "Stressed mirror polishing. 1: A technique for producing nonaxisymmetric mirrors," Appl. Opt. **19,** 2332–2340 (1980).
7. J. E. Shigley and C. R. Mischke, *Mechanical Engineering Design,* 5th ed. (McGraw-Hill, New York, 1989), Chap. 7, pp. 269–303.
8. S. C. West and W. B. Davison, "Fatigue limits of a 2.2m stressed lap baseplate on the MMT and Columbus mirrors," Multiple Mirror Telescope Conversion Tech. Mem. **92-3** (University of Arizona, Tucson, Ariz., 1992).